

Coherent Population Trapping with High Common-Mode Noise Rejection Using Differential Detection of Simultaneous Dark and Bright Resonances

Peter Yun (云恩学)^{1,*}, Rodolphe Boudot,² and Emeric de Clercq³

¹ National Time Service Center, Chinese Academy of Sciences, Xi'an 710600, People's Republic of China

² FEMTO-ST, CNRS, Université de Franche-Comté, SupMicrotech-ENSMM, 26 rue de l'épitaphe, 25030 Besançon, France

³ Systèmes de Référence Temps-Espace (SYRTE), Observatoire de Paris, 75014 Paris, France



(Received 18 July 2022; revised 3 November 2022; accepted 22 December 2022; published 3 February 2023)

Coherent manipulation of atomic states is highly desirable in numerous applications spanning from fundamental physics to metrology. In this study, we propose and demonstrate, theoretically and experimentally, the simultaneous observation in a vapor cell of dark and bright resonances that provide, through a differential-detection stage, an output coherent-population-trapping atomic resonance that benefits from a doubled amplitude and high common-mode noise rejection. This advanced spectroscopic scheme might be of interest for the development of high-performance vapor-cell atomic clocks, sensors, or high-resolution spectroscopy experiments.

DOI: 10.1103/PhysRevApplied.19.024012

I. INTRODUCTION

The driving of two atomic transitions that share a common excited level with a coherent bichromatic light field in a Λ scheme yields, through electromagnetically induced transparency (EIT) [1], the detection of a narrow atomic resonance line at the output of the atomic medium. This spectroscopic feature, explained by coherent population trapping (CPT) [2–4] of atoms into a quantum dark state [5], can exhibit a line width several orders of magnitude lower than the natural line width of the optical transitions. CPT has been implemented in a plethora of applications, including the demonstration of compact [6–9] and miniaturized cell-based atomic clocks [10], optical frequency references [11–13], magnetometers [14], atom-laser cooling [15,16], quantum information science [17], and slow-light experiments [18].

The counterpart effect to EIT is electromagnetically induced absorption (EIA). This phenomenon, reported in Ref. [19] and initially explained in Ref. [20], can be also observed in three-level Λ systems by using two counter-propagating bichromatic light fields with properly chosen polarizations and mutual phase delay, such that a dark state created by one dual-frequency light field is a bright state for the other [21]. The detection of two-photon EIA resonances has recently been applied for the demonstration of a vapor-cell atomic clock [22] or combined with

pulsed interrogation for the observation of subkilohertz Ramsey-narrowed EIA resonances [23].

CPT and EIA-based vapor-cell atomic clocks have demonstrated short-term fractional frequency stability levels, at 1 s integration time, in the low- 10^{-13} range [6,8,9] and at 4×10^{-12} , respectively [22]. Although remarkable, this performance remains about one order of magnitude worse than the ultimate photon shot-noise limit [24], i.e., at the level of a few $10^{-14} \tau^{-1/2}$ (where τ is the integration time). Thus it is of crucial importance to propose innovative CPT pumping schemes that might tackle this remaining obstacle. In CPT spectroscopy, numerous optimized double- Λ schemes have been proposed to increase the CPT signal [25–33]. In addition, several differential-detection schemes have been proposed to mitigate the laser noise that usually pollutes the resonance signal [34–36].

In this work, we propose and demonstrate a method for the detection of coherent superposition-state resonances with an enhanced signal-to-noise ratio (SNR) through the simultaneous detection of EIT and EIA resonances and a subsequent differential-detection stage. Initially prepared into a CPT state that can employ various interaction schemes [25–27,30,32], atoms are then interrogated with a finely phase-delayed linearly polarized bichromatic probe beam, such that the initial CPT state is a dark state or bright state for respective orthogonal circularly polarized components of the probe field. Explained by the fact that one of the four electric dipole moments involved in the double- Λ system of the alkali-atom D_1 line is of opposite sign to the other three, EIT and EIA resonances are then simultaneously generated. These two orthogonally

*Corresponding author: yunenxue@ntsc.ac.cn; permanent e-mail: yunenxue@163.com

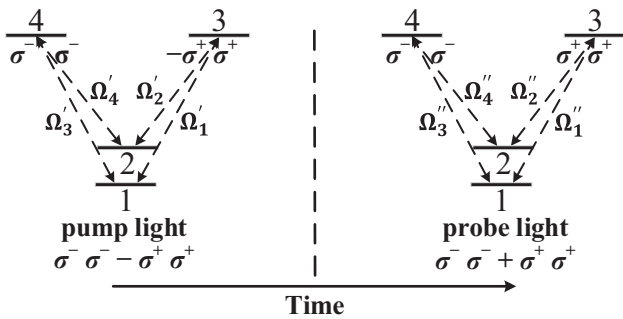


FIG. 1. The principle of the double- Λ four-level system, coupled successively with the pump and probe light. Note the sign difference of one σ^+ polarization component between the pump and the probe light.

polarized signals are then optically separated at the cell output and subtracted from each other, yielding an output signal with an enhanced amplitude and suppressed common noise. The experimental results are explained well by a dedicated model and may be a promising step toward the demonstration of a high-performance vapor-cell CPT clock.

II. BASIC THEORY

The principle of our approach is depicted in Fig. 1. The interaction Hamiltonian of the simplified four-level atomic scheme is [32]

$$\begin{aligned} V_1 &= V_{1+} + V_{1-} \\ &= \frac{-\hbar}{2} (\Omega'_1 |3\rangle\langle 1| + \Omega'_2 |3\rangle\langle 2| + \text{H.C.}) \\ &\quad + \frac{-\hbar}{2} (\Omega'_3 |4\rangle\langle 1| + \Omega'_4 |4\rangle\langle 2| + \text{H.C.}), \end{aligned} \quad (1)$$

where ‘‘H.C.’’ denotes the Hermitian conjugate, $\Omega'_{3(4)} = \Omega e^{i\phi'_{3(4)}}$, $\Omega'_1 = \Omega e^{i\phi'_1}$, and $\Omega'_2 = -\Omega e^{i\phi'_2}$. We note that $\Omega = d\mathcal{E}_0/\hbar$ is the Rabi frequency, in which d is the electric dipole matrix element of the transition, and \mathcal{E}_0 the amplitude of the laser electric field. The minus sign in the last term is due to the opposite sign of its electric dipole moment, compared to the other three, such that $-d_{23} = d_{24} = d_{13} = d_{14} = d$, and ϕ'_i ($i=1,\dots,4$) are the phases of each frequency component.

In the rotating frame and at resonance, the dark and bright states prepared by one circularly polarized (say, σ^+) bichromatic light beam can be written, respectively, as

$$\begin{aligned} |d_{1+}\rangle &= \cos \theta_+ |1\rangle - \sin \theta_+ |2\rangle, \\ |b_{1+}\rangle &= \sin^* \theta_+ |1\rangle + \cos^* \theta_+ |2\rangle, \end{aligned} \quad (2)$$

where $\sin \theta_+ = \Omega'_1 / \sqrt{|\Omega'_1|^2 + |\Omega'_2|^2}$, $\cos \theta_+ = \Omega'_2 / \sqrt{|\Omega'_1|^2 + |\Omega'_2|^2}$. Similarly, we can write the dark, $|d_{1-}\rangle$,

and bright, $|b_{1-}\rangle$, states for the counter-rotating circularly polarized (σ^-) bichromatic light beam. Each dark state is decoupled from its pump light, i.e., $\langle 3 | V_{1+} | d_{1+} \rangle = 0$ and $\langle 4 | V_{1-} | d_{1-} \rangle = 0$.

In our study, atoms are prepared in a CPT state using a double- Λ system obtained with the push-pull optical pumping (PPOP) scheme [25,26]. In this scheme, a Michelson system is employed to introduce a phase delay and compensate the opposite sign of d_{23} , i.e., $\phi'_+ = \phi'_- + (2p_1 + 1)\pi$, with $\phi'_{+(-)} = \phi'_{1(3)} - \phi'_{2(4)}$, and p_i ($i=1-4$) is an arbitrary integer. The atom-light interaction for pumping the atoms in the CPT state is then denoted $\sigma^- \sigma^- - \sigma^+ \sigma^+$, as shown in Fig. 1. In this configuration, we arrive, with an appropriate phase, at $|d_{1+}\rangle = |d_{1-}\rangle \equiv |d_1\rangle$, meaning that each dark state built by one circular polarization is also a dark state for the counter-rotating polarization.

In the second step, shown in Fig. 1, the atomic ensemble is probed by a linearly polarized bichromatic beam. Since the σ^+ and σ^- polarization components of this field are in phase in this case, i.e., $\phi'_+ = \phi'_- + 2p_2\pi$, with $\phi'_{+(-)} = \phi'_{1(3)} - \phi'_{2(4)}$, the dark states previously created, $|d_1\rangle$, will be coupled to or uncoupled from the probe light, depending on whether the interaction field is σ^+ or σ^- polarized. The interaction of the atomic ensemble with the probe field is denoted $\sigma^- \sigma^- + \sigma^+ \sigma^+$, as shown in Fig. 1.

The interaction Hamiltonian for the σ^+ component of the probe beam is

$$V_{2+} = \frac{-\hbar}{2} (\Omega''_1 |3\rangle\langle 1| + \Omega''_2 |3\rangle\langle 2| + \text{H.C.}) \quad (3)$$

A proper phase-delay setting between the probe and pump light, e.g., $\phi'_+ - \phi''_+ = 2p_3\pi$, leads to $V_{2+} |d_1\rangle = 0$. In this case, the previous dark state remains a dark state and EIT is observed. At the opposite, for the σ^- component, the reverse applies, since $\phi'_- - \phi''_- = (2p_4 + 1)\pi$, leading to $V_{2-} |d_1\rangle \neq 0$. In this case, the previous dark state becomes a bright state and EIA occurs.

Based on this four-level model, we also perform numerical calculations using the Liouville equation (see the Appendix). Figure 2 shows the calculated signals at both outputs of a polarizing beam splitter (PBS) placed at the cell output. The figure clearly demonstrates the simultaneous presence of EIT and EIA resonances detected at null Raman detuning. Once obtained, a differential CPT signal can be obtained by subtracting the EIA from the EIT signal. We note here that our scheme, in comparison with previously reported differential-detection schemes [34–36], offers ideal differential detection with a doubled amplitude of the signal and rejection of the common-mode noise.

III. EXPERIMENTAL SETUP

Using this concept, the experimental setup depicted in Fig. 3, based on that described in Ref. [9], is implemented.

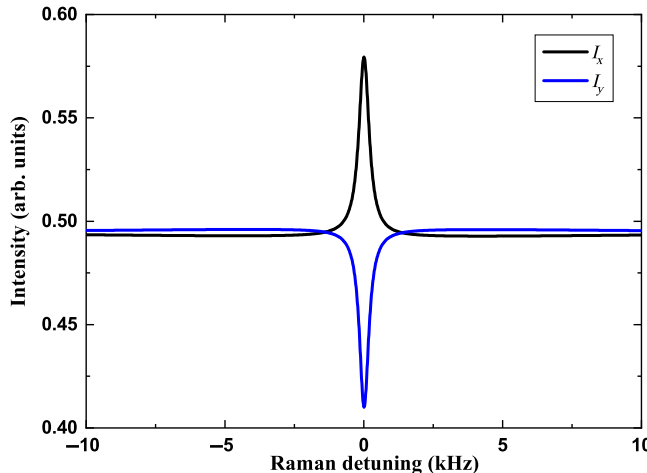


FIG. 2. The transmitted light signals obtained by theoretical calculation. I_x and I_y are the intensities on the two orthogonal polarization axes. The parameter values are the Rabi frequency $\Omega/(2\pi) = 0.06$ MHz, the excited-state to ground-state decay rate $\Gamma/(2\pi) = 0.6$ GHz, the ground-state coherence decay rate $\gamma_2/(2\pi) = 200$ Hz, the electric field ratio of probe to pump beam $k_0 = 1/\sqrt{2}$, $\tau_1 = 4.5$ ms, $t_d = 4.502$ ms, and $t_w = 30 \mu\text{s}$. The parameters of the time sequence are defined in Fig. 3.

A distributed-Bragg-reflector (DBR) laser is directly modulated at 3.417 GHz in order to produce a multifrequency laser field, such that both first-order optical sidebands are used for CPT interaction. The light beam is then separated into three arms. The first arm is used to stabilize the laser carrier frequency to the midpoint of the two transitions of the ^{87}Rb D_1 line, i.e., $|5^2S_{1/2}, F=1\rangle \rightarrow |5^2P_{1/2}, F'=2\rangle$ and $|5^2S_{1/2}, F=2\rangle \rightarrow |5^2P_{1/2}, F'=2\rangle$, using dual-frequency sub-Doppler spectroscopy [11] in a vacuum reference cell. The second arm is directed to a Michelson system in order to produce two phase-delayed counter-rotating circularly polarized dual-frequency light fields and then to generate the PPOP scheme used as the pumping field. The third arm is used to prepare the probing light field. The latter is properly phase delayed relative to one arm of the Michelson interferometer, while a half-wave plate is used to tune its polarization plane. The pump and probe beams are overlapped with the aid of a nonpolarizing beam splitter (BS). Two acousto-optic modulators (AOMs), both driven at 180 MHz, are used to switch the pump and probe lights on and off. These AOMs also compensate for the buffer-gas-induced optical frequency shift in the clock cell. The pump and probe beams are expanded to a circular beam with a $1/e^2$ diameter of about 5 mm before the clock cell. The ^{87}Rb -isotope-enriched cylindrical vapor cell (diameter 20 mm, length 50 mm) is filled with a $\text{N}_2\text{-Ar}$ buffer-gas mixture and temperature stabilized at around 54.6 °C. Unless otherwise specified, a uniform axial static magnetic field, $B_0 = 14.6 \mu\text{T}$, is applied to increase the Zeeman degeneracy. The ensemble

is surrounded by one layer of mu-metal magnetic shield. At the cell output, the transmitted light is polarization rotated by $\pi/4$ with respect to the axis of the following polarizing beam splitter (PBS), then separated into two paths by the PBS, and finally detected by balanced photodetectors (PDs).

The pump and probe light beams interact with the atomic ensemble in the sequence shown in Fig. 3(b), where T_c is the cycle time. Atoms are first prepared in CPT states during a pumping stage of length τ_1 , usually of several milliseconds. At the end of this pumping stage, a probing-light window of length τ_2 , much smaller than τ_1 , is opened. The PD signals are then recorded during a short detection window of length t_w , in the range of 30–100 μs , which, after a delay time of 2 μs , follows the probe-light activation. In our system, the detection window time is tuned such that $0 < t_w \leq \tau_{\text{deph}} \leq \tau_2$, where $\tau_{\text{deph}} \approx 1$ ms in our experiment is the time for the two previously prepared dark states to become common bright states and interact with each other. Ramsey-CPT interrogation can be also performed by inserting a free-evolution dark time, of length T , between the end of the pumping window and the start of the probing window.

IV. EXPERIMENTAL RESULTS

Figure 4 shows typical simultaneously observed EIT, EIA, and differential-CPT (diff-CPT) experimental signals. Narrow-line-width and high-contrast (14.4%) EIT and EIA signals are obtained. The three peaks correspond to respective $\Delta m_F = 0$ transitions between sublevels of the magnetic quantum number $m_F = -1, 0, +1$, respectively, with the central peak being the clock transition. The amplitude asymmetry of the lateral peaks ($m_F = \pm 1$) between the EIT and EIA signals can be explained by a residual elliptic polarization and optical pumping effects. Indeed, the σ^- component of the probe beam, for which the previously created dark states are now bright states, pumps atoms toward lower-magnetic-number Zeeman sublevels, whereas the σ^+ component, for which the previously created dark states remain dark, pumps atoms toward higher-magnetic-number Zeeman sublevels. Compared to the EIT and EIA signals, the diff-CPT signal is detected with a dc background level that is almost nulled and its amplitude is 2 times higher. This configuration is then favorable for achieving a CPT resonance with high contrast (usually defined as the ratio between the resonance amplitude and its dc background level). The line width of the diff-CPT signal is between those of the EIT and EIA resonances. More importantly, the common-mode noise is highly rejected, as better highlighted in the following section.

We measure the dependence of the resonance amplitude, the line width [full width at half maximum (FWHM)], and the SNR-to-FWHM ratio on the laser pump power,

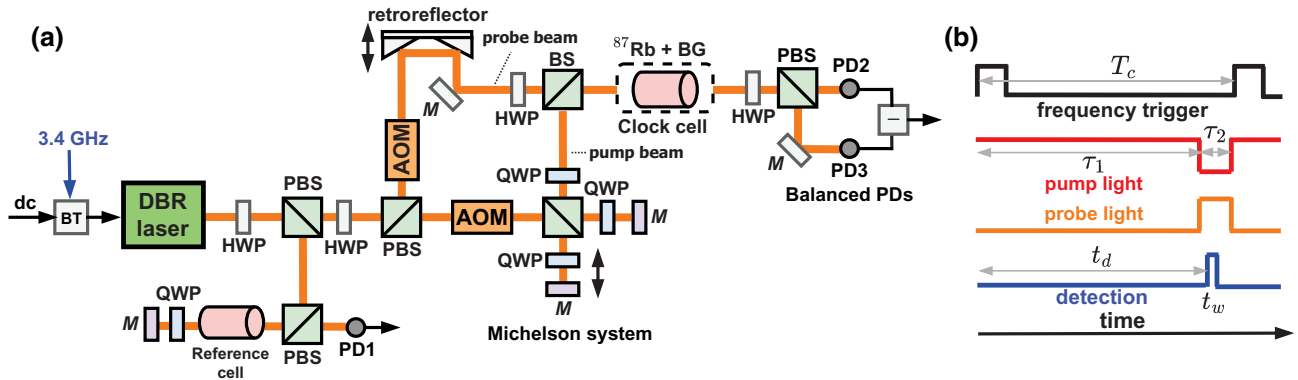


FIG. 3. (a) The experimental setup. BS, nonpolarizing beam splitter; PBS, polarizing beam splitter; PD, photodetector; AOM, acousto-optic modulator; QWP, quarter-wave plate; HWP, half-wave plate; M, mirror; BT, bias tee. (b) The time sequence for CPT spectroscopy.

for the EIT, EIA, and diff-CPT signals. Here, the SNR is defined as $\text{SNR} = A_{\text{CPT}}/N$, where A_{CPT} is the CPT amplitude (the difference between the CPT value at resonance and the Doppler-broadened absorption background), while the noise N is the typical fluctuation at 1 s of the signal measured at half maximum of the detected CPT resonance [37]. The results are shown in Fig. 5. The line width increases with the pump power, while the amplitude saturates for powers higher than about 350 μW . The SNR-to-FWHM ratio is maximized for laser powers lower than 50 μW . This ratio is more than 3 times higher in the case

of the diff-CPT signal, in the region of interest. We perform a comparable test as a function of the laser probe power. In this case, we find that the line width remains about constant, while the amplitude increases for all cases. The SNR-to-FWHM ratio is maximized at a probe power of 48 μW .

An important feature of the proposed spectroscopic approach is the expected rejection of the common-mode noise on the differential CPT signal. This property is clearly demonstrated in Fig. 6, in the case of a measurement at low laser power (here, 6 μW). In this configuration, the SNR of the diff-CPT signal is improved by a factor of almost 10, in comparison with those obtained for the initial EIT and EIA signals. We observe that the noise mitigation obtained with the proposed method is better here,

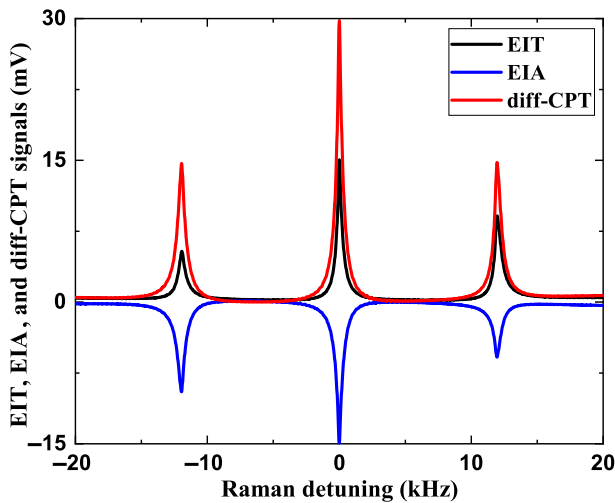


FIG. 4. Experimentally observed EIT, EIA, and diff-CPT signals. The experimental parameters are as follows: $T_c = 3.1$ ms, $\tau_1 = 3$ ms, $\tau_2 = 0.1$ ms, $t_d = 3.002$ ms, $t_w = 0.03$ ms, $B_0 = 0.87$ μT , $P_{\text{pump}} = 107$ μW , and $P_{\text{probe}} = 57$ μW . Offsets of 103.2 and 103.4 mV are subtracted from the EIT and EIA signals, respectively. The diff-CPT signal is detected with a dc background level that is almost nulled and exhibits an amplitude that is 2 times higher than those of the EIA and EIT resonances. This figure shows the outputs of the photodiodes in working conditions, with both PD2 and PD3 illuminated by incident light.

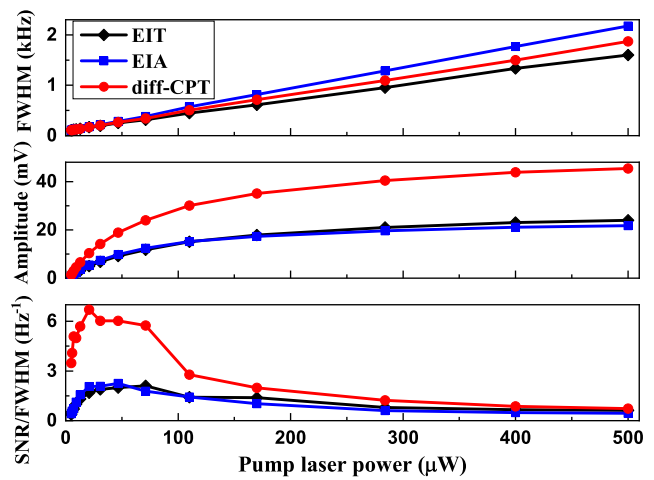


FIG. 5. The signal line width, amplitude, and SNR-to-FWHM ratio of the EIT, EIA, and diff-CPT amplitudes as a function of the laser pump power. The experimental parameters are as follows: $T_c = 4.6$ ms, $\tau_1 = 4.5$ ms, $\tau_2 = 0.1$ ms, $t_d = 4.502$ ms, $t_w = 0.03$ ms, and $P_{\text{probe}} = 57$ μW . The solid lines are guides to the eye.

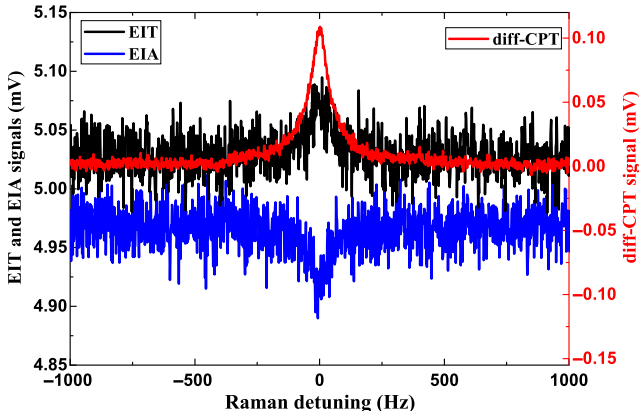


FIG. 6. The EIT, EIA, and diff-CPT signals obtained for a low-laser-power record. The experimental parameters are as follows: $T_c = 4.6$ ms, $\tau_1 = 4.5$ ms, $\tau_2 = 0.1$ ms, $t_d = 4.502$ ms, $t_w = 0.03$ ms, $P_{\text{pump}} = 6.1 \mu\text{W}$, and $P_{\text{probe}} = 5.9 \mu\text{W}$. For this plot, the EIA is down shifted for clarity. The SNR of the diff-CPT signal is about 10 times higher than for the EIT and EIA signals.

at low power, than that obtained at a higher power [see Fig. 5]. This dependence on the laser power of the noise mitigation factor is not clear to date and will be investigated in a dedicated future study. We also note that in Fig. 6, the diff-CPT resonance exhibits a narrow line width of 97 Hz.

For further investigation, we also measure the noise spectrum of the error signal when a local oscillator (LO) is locked to the atomic resonance [38]. In this evaluation, we use a standard synchronous modulation-demodulation technique of the microwave frequency, with a frequency-modulation (FM) depth of about 85 Hz and a FM period of $T_{\text{FM}} = 2 T_c$, to generate an error signal that might be used to stabilize the LO frequency. The noise spectrum of the error signal is then measured in closed-loop operation of the atomic clock with a noise analyzer (Stanford Research Systems, SR785). Noise spectra obtained for the EIT, EIA, and diff-CPT error signals, as well as the error signals themselves, are shown in Fig. 7.

In the noise spectra shown in Fig. 7, the noise valleys at 13.6 Hz and its harmonics are suspected to come from the feedback rate $1/T_{\text{FB}}$, with one feedback applied every eight FM-cycle periods, i.e., $T_{\text{FB}} = 8 T_{\text{FM}}$. Most importantly, the noise level of the diff-CPT error signal is highly reduced. This result suggests that our method should help to improve the performance of CPT clocks, including those based on push-pull optical pumping [39,40], dominated by laser AM-AM and FM-AM noise sources (where AM refers to amplitude modulation). Specifically, here, the noise amplitude of the diff-CPT signal is divided by 4.5 compared to the EIT and EIA cases in the 1 Hz to 1 kHz offset range. Thus, the frequency stability of the atomic clock using the diff-CPT signal should be about 4.5 times better than one based on EIT or EIA signals.

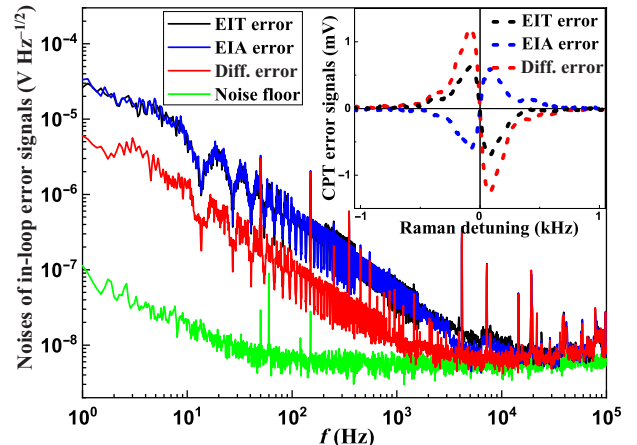


FIG. 7. The noise of the in-loop error signals, for the EIT, EIA, and diff-CPT cases. The experimental parameters are as follows: $T_c = 4.61$ ms, $\tau_1 = 4.5$ ms, $\tau_2 = 0.11$ ms, $t_d = 4.502$ ms, $t_w = 0.1$ ms, $P_{\text{pump}} = 30.7 \mu\text{W}$, and $P_{\text{probe}} = 11.8 \mu\text{W}$. The noise floor of the analyzer is also plotted for information. The inset shows the EIT, EIA, and diff-CPT error signals with the same conditions.

We also observe the spectral line shape of $|F = 1, m_F = \pm 1\rangle \leftrightarrow |F = 2, m_F = \mp 1\rangle$ transitions in the present configuration. These $\Delta m_F = \pm 2$ transitions, shown in Fig. 8, are well separated from the clock transition at a “high” magnetic field (here, $B_0 = 233 \mu\text{T}$). Their shape is different from those observed in Refs. [26,41]. For $\Delta m_F = -2$, an EIT signal is observed for the clock-transition EIT channel, while an EIA signal is obtained in the clock-transition EIA channel. In the case of $\Delta m_F = +2$, the

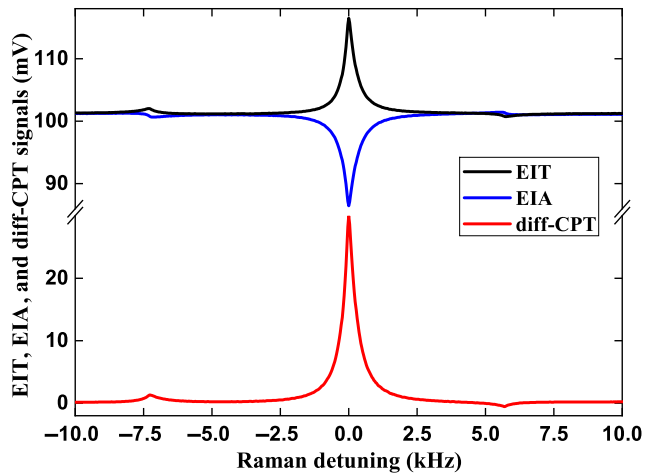


FIG. 8. EIT, EIA, and diff-CPT signals with $\Delta m_F = 0$ and $\Delta m_F = \pm 2$. The experimental parameters are as follows: $T_c = 4.6$ ms, $\tau_1 = 4.5$ ms, $\tau_2 = 0.1$ ms, $t_d = 4.502$ ms, $t_w = 0.03$ ms, $P_{\text{pump}} = 107 \mu\text{W}$, and $P_{\text{probe}} = 57 \mu\text{W}$. The static magnetic field is $B_0 = 233 \mu\text{T}$. Here, the clock transition is shifted by 3.128 kHz in comparison with previous cases, due to the second-order Zeeman shift.

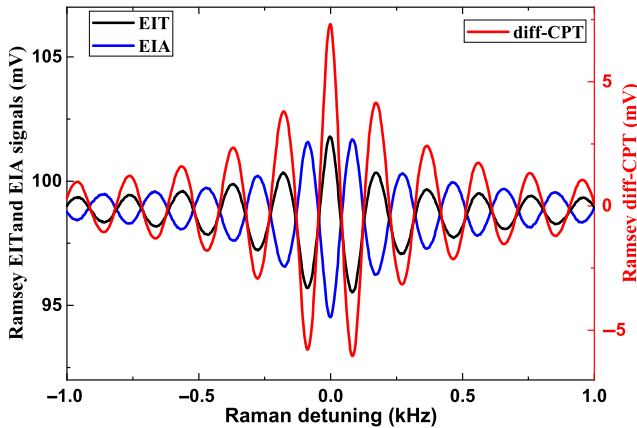


FIG. 9. The Ramsey EIT, EIA, and diff-CPT signals. The experimental parameters are as follows: $T_c = 9.6$ ms, $\tau_1 = 4.5$ ms, $T = 5$ ms, $\tau_2 = 0.1$ ms, $t_d = 9.502$ ms, $t_w = 0.03$ ms, $P_{\text{pump}} = 107 \mu\text{W}$, and $P_{\text{probe}} = 57 \mu\text{W}$.

reverse applies. Again, here, the differential signal, i.e., the EIT channel minus the EIA channel, shows a higher SNR. This observation shows that our method can also be applied to the lin||lin CPT scheme [28]. To apply this idea, both the pump and probe beams should be linearly polarized, with the probe-beam polarization axis rotated by 45° relative to the pump-light polarization. If one of the two polarization components of the probe beam—say, on the x axis—induces EIT, the orthogonal component will induce EIA. With a similar polarization separation, we can then simultaneously observe EIT, EIA, and differential CPT signals in the lin||lin scheme.

Finally, we succeed in detecting experimental Ramsey fringes of EIT, EIA, and diff-CPT by applying a pulsed interrogation sequence. Similarly to other Ramsey-CPT clocks [27,40], this regime is obtained by inserting a free-evolution dark time, of length T , between the end of the pumping window and the start of the probing window. The EIT, EIA and diff-CPT Ramsey fringes thus obtained, with $T = 5$ ms, are shown in Fig. 9.

A narrow fringe line width of 78.2 Hz is observed for $T = 5$ ms. Here again, we note that the amplitude of the central fringe is doubled in the case of the diff-CPT signal. For information, we measure the CPT coherence relaxation time T_2 for each channel, by varying the Ramsey time T . We find T_2 coherence times of 4.4 ± 0.04 ms, 5.33 ± 0.25 ms, and 4.88 ± 0.11 ms for the EIT, EIA, and diff-CPT signals, respectively.

V. CONCLUSIONS

In conclusion, we propose and demonstrate, theoretically and experimentally, a spectroscopic approach for simultaneous observation of EIT and EIA signals in a single atomic ensemble. Subsequent extraction of a differential signal at the cell output allows the detection of a CPT

resonance with a doubled amplitude and high common-mode noise rejection. This method relies on the use of double- Λ schemes for which one of the four involved dipolar moments is of opposite sign to the others. This method is then quite universal, because the pumping light can make use of various optimized CPT pumping schemes [25–32], including the lin || lin scheme [28], and can be also applied to other alkali-metal atoms. The proposed approach might be of great interest in the development of a high-performance CPT clock, possibly surpassing the state-of-the-art stability results of current CPT clocks [6,8,9] and approaching the long-sought-after level of a few $10^{-14}\tau^{-1/2}$ predicted by the photon shot-noise limit [24].

ACKNOWLEDGMENTS

We gratefully acknowledge Thomas Zanon-Willette (Sorbonne Université), Moustafa Abdel Hafiz (FEMTO-ST), and James McGilligan (University of Strathclyde) for careful reading of the manuscript and constructive suggestions. This work was funded by the National Natural Science Foundation of China (Grants No. 12173043 and No. U1731132). R.B. was supported by Région Bourgogne Franche-Comté in the frame of the HACES project and by the LabeX FIRST-TF (Grant No. ANR 10-LABX-0048).

APPENDIX: THEORETICAL SIMULATION

In this appendix, we show how the EIT and EIA signals occur simultaneously. This study is extracted from theoretical simulations based on the four-level model shown in Fig. 1, using the Liouville equation and the polarization-rotation calculation method.

1. The pump and probe light fields

The bichromatic light is described by a classical field with angular frequency ω_\pm , propagating along the z axis. The electric field of the pump light can be represented by

$$\mathbf{E}_{\text{pump}} = \mathcal{E}_0 f_a(t) \{ [\cos(\omega_+ t + \phi'_1) + \cos(\omega_- t + \phi'_2)] \hat{\mathbf{e}}_+ + [\cos(\omega_+ t + \phi'_3) + \cos(\omega_- t + \phi'_4)] \hat{\mathbf{e}}_- \}. \quad (\text{A1})$$

During the probe stage, the linearly polarized probe beam, with a polarization angle θ relative to the x axis, can be written as

$$\mathbf{E}_{\text{probe}} = k_0 \mathcal{E}_0 f_b(t) [\cos(\omega_+ t + \phi''_3) + \cos(\omega_- t + \phi''_4)] \hat{\mathbf{e}}_\theta. \quad (\text{A2})$$

Here, k_0 is the amplitude ratio between the pump and probe electric fields, $f_a(t) = U[t] - U[t - \tau]$, and $f_b(t) = f_a(t - \tau)$, where $U[t]$ is a step function. In order to take the switching times ($1 \mu\text{s}$) of the pump and probe beams

into account in our experiments, a sine function is used to replace the rising and falling edges of the step function.

With the definitions $\hat{e}_\theta = (\cos \theta \hat{e}_+ + \sin \theta \hat{e}_-) / \sqrt{2}$, $\hat{e}_x = -(\hat{e}_+ - \hat{e}_-) / \sqrt{2}$, and $\hat{e}_y = i(\hat{e}_+ + \hat{e}_-) / \sqrt{2}$, we can rewrite as follows:

$$\begin{aligned} \mathbf{E}_{\text{probe}} &= k_0 \mathcal{E}_0 f_b(t) \\ &\quad \{ [\cos(\omega_+ t + \phi_1'') + \cos(\omega_- t + \phi_2'')] e^{-i\theta} \hat{e}_+ \\ &\quad + [\cos(\omega_+ t + \phi_3'') + \cos(\omega_- t + \phi_4'')] e^{i\theta} \hat{e}_- \} / \sqrt{2}, \end{aligned} \quad (\text{A3})$$

where $\phi_{1(2)}'' = \phi_{3(4)}'' + m(n)\pi$, in which m and n are arbitrary odd integers.

2. Polarization rotation of the clock-cell transmitted light

Using the Jones matrix and with $\hat{e}_\pm = \mp(\hat{e}_x \pm i\hat{e}_y) / \sqrt{2}$, the electric field [Eq. (A3)] of the probe beam can be written as

$$\mathbf{E}_{\text{probe}} = \frac{k_0 \mathcal{E}_0}{\sqrt{2}} \sum_{\omega_\pm}^{\omega_-} \left\{ e^{-i\theta} \begin{bmatrix} -1 \\ -i \end{bmatrix}_{\omega_+} + e^{i\theta} \begin{bmatrix} 1 \\ -i \end{bmatrix}_{\omega_+} \right\}. \quad (\text{A4})$$

From Refs. [42–44], we know that when the probe beam is transmitted across the clock cell with length L , it is changed to

$$\mathbf{E}_1 = \frac{k_0 \mathcal{E}_0}{\sqrt{2}} \sum_{\omega_\pm}^{\omega_-} \left\{ e^{-i\theta + \xi_{\omega_\pm}^+} \begin{bmatrix} -1 \\ -i \end{bmatrix}_{\omega_+} + e^{i\theta + \xi_{\omega_\pm}^-} \begin{bmatrix} 1 \\ -i \end{bmatrix}_{\omega_+} \right\}, \quad (\text{A5})$$

with $\xi_{\omega_\pm}^\pm = -i\beta_{\omega_\pm}^\pm - \alpha_{\omega_\pm}^\pm L/2$ and $\beta_{\omega_\pm}^\pm = 2\pi L n_{\omega_\pm}^\pm / \lambda_{\pm}$, where $n_{\omega_\pm}^\pm$ are the refractive indices of the ^{87}Rb atomic medium for the components that are left and right circularly polarized and $\alpha_{\omega_\pm}^\pm$ are the corresponding absorption coefficients.

Thus, by placing, at the cell output, a half-wave plate characterized by its Jones matrix

$$W_{\lambda/2} = -i \begin{bmatrix} \cos 2\psi & \sin 2\psi \\ \sin 2\psi & -\cos 2\psi \end{bmatrix}, \quad (\text{A6})$$

we can rotate the polarization of the field \mathbf{E}_1 through an angle $2\psi = \pi/4 - \theta$. Thus, we obtain the output probe beam with its polarization set to an angle $\pi/4$ relative to the x axis, for the balance of the two PDs. It reads as

follows:

$$\begin{aligned} \mathbf{E}_2 &= W_{\lambda/2} \mathbf{E}_1 = \frac{-ik_0 \mathcal{E}_0}{\sqrt{2}} \\ &\quad \sum_{\omega_\pm}^{\omega_-} \left\{ e^{-i\theta + \xi_{\omega_\pm}^+} \begin{bmatrix} -e^{i2\psi} \\ ie^{i2\psi} \end{bmatrix}_{\omega_+} + e^{i\theta + \xi_{\omega_\pm}^-} \begin{bmatrix} e^{-i2\psi} \\ ie^{-i2\psi} \end{bmatrix}_{\omega_+} \right\}. \end{aligned} \quad (\text{A7})$$

Thus, for the x -axis polarization detection, with $I_0 = \varepsilon_0 (k_0 \mathcal{E}_0)^2$, we have

$$I_x = \frac{I_0}{2} \sum_{\omega_\pm}^{\omega_-} [e^{-\alpha_{\omega_\pm}^+ L} + e^{-\alpha_{\omega_\pm}^- L} - 2 \sin(4\theta + 2\beta_{\omega_\pm}) e^{-\alpha_{\omega_\pm} L}]. \quad (\text{A8})$$

Similarly, for the y -axis polarization detection, we have

$$I_y = \frac{I_0}{2} \sum_{\omega_\pm}^{\omega_-} [e^{-\alpha_{\omega_\pm}^+ L} + e^{-\alpha_{\omega_\pm}^- L} + 2 \sin(4\theta + 2\beta_{\omega_\pm}) e^{-\alpha_{\omega_\pm} L}], \quad (\text{A9})$$

in which $\beta_{\omega_\pm} = (\beta_{\omega_\pm}^+ - \beta_{\omega_\pm}^-)/2$, $\beta_{\omega_\pm}^\pm = 2\pi L n_{\omega_\pm}^\pm / \lambda_{\pm}$, $n_{\omega_\pm}^\pm = \sqrt{1 + \text{Re}(\chi_{\omega_\pm}^\pm)}$, $\alpha_{\omega_\pm} = (\alpha_{\omega_\pm}^+ + \alpha_{\omega_\pm}^-)/2$, $\alpha_{\omega_\pm}^\pm = 2\pi \text{Im}(\chi_{\omega_\pm}^\pm) / \lambda_{\pm}$, and $\chi_{\omega_\pm}^\pm$ are the susceptibilities of the atomic medium.

3. Liouville equations

The four-level system shown in Fig. 1 is adopted. The evolution of the density matrix for atoms at rest is given by the Liouville equation,

$$\dot{\rho} = \frac{-i}{\hbar} [H, \rho] - R\rho, \quad (\text{A10})$$

where $H = H_0 + V$, $H_0 = \hbar \sum_{i=1}^4 \omega_i |i\rangle \langle i|$ is the Hamiltonian of the unperturbed atom, and ω_i is the angular frequency for level $|i\rangle$. R is the relaxation matrix. The interaction Hamiltonian is $V = -\mathbf{D} \cdot (\mathbf{E}_{\text{pump}} + \mathbf{E}_{\text{probe}})$, with \mathbf{D} the electric dipole operator. It reads

$$\begin{aligned} V &= V_+ + V_- = \frac{-\hbar}{2} (\Omega_1 |3\rangle \langle 1| + \Omega_2 |3\rangle \langle 2| + \text{H.C.}) \\ &\quad + \frac{-\hbar}{2} (\Omega_3 |4\rangle \langle 1| + \Omega_4 |4\rangle \langle 2| + \text{H.C.}), \end{aligned} \quad (\text{A11})$$

where $\Omega_{1(2)} = \mathcal{E}_0 f_{1(2)}(t) \vec{d}_{1(2)3} \hat{e}_+ / \hbar$, $\Omega_{3(4)} = \mathcal{E}_0 f_{3(4)}(t) \vec{d}_{1(2)4} \hat{e}_- / \hbar$, $f_j(t) = f_a(t) e^{-i\phi_j} + k_0 f_b(t) e^{-i\varphi_j}$, $j = 1-4$, $\varphi_{1(2)} = \phi_{1(2)}'' + \theta$, and $\varphi_{3(4)} = \phi_{3(4)}'' - \theta$.

For simplicity and without loss of generality, we assume that $\phi'_1 = \phi'_2 = \phi'_3 = 0$, $\phi'_4 = \pi$, and $\phi''_1 = \phi''_2 = \pi$, $\phi''_3 =$

$\phi_4'' = 0$. This leads to $f_1(t) = f_2(t) = f_a(t) - k_0 f_b(t) e^{-i\theta}$, $f_3(t) = f_a(t) + k_0 f_b(t) e^{i\theta}$, and $f_4(t) = -f_a(t) + k_0 f_b(t) e^{i\theta}$;

thus, we have $\Omega_1 = -\Omega_2 = \Omega f_1(t)$, $\Omega_3 = \Omega f_3(t)$, and $\Omega_4 = \Omega f_4(t)$.

The density-matrix evolution is given by

$$\begin{aligned} \dot{\rho}_{11} &= \Omega \operatorname{Im}(\tilde{\rho}_{13} f_1(t)) + \Omega \operatorname{Im}(\tilde{\rho}_{14} f_3(t)) + (\rho_{33} + \rho_{44})\Gamma/2 - (\rho_{11} - \rho_{22})\gamma_1, \\ \dot{\rho}_{22} &= -\Omega \operatorname{Im}(\tilde{\rho}_{23} f_2(t)) + \Omega \operatorname{Im}(\tilde{\rho}_{24} f_4(t)) + (\rho_{33} + \rho_{44})\Gamma/2 - (\rho_{22} - \rho_{11})\gamma_1, \\ \dot{\rho}_{33} &= -\Omega \operatorname{Im}(\tilde{\rho}_{13} f_1(t)) + \Omega \operatorname{Im}(\tilde{\rho}_{23} f_2(t)) - \rho_{33}\Gamma, \\ \dot{\rho}_{44} &= -\Omega \operatorname{Im}(\tilde{\rho}_{14} f_3(t)) - \Omega \operatorname{Im}(\tilde{\rho}_{24} f_4(t)) - \rho_{44}\Gamma, \\ \dot{\tilde{\rho}}_{14} &= i[(i\Gamma - 2\pi\Delta)\tilde{\rho}_{14} + (\rho_{44} - \rho_{11})\Omega f_3^*(t) - \tilde{\rho}_{12}\Omega f_4^*(t) + \rho_{34}\Omega f_1^*(t)]/2, \\ \dot{\tilde{\rho}}_{13} &= i[(i\Gamma - 2\pi\Delta)\tilde{\rho}_{13} + (\rho_{33} - \rho_{11})\Omega f_1^*(t) + \tilde{\rho}_{12}\Omega f_2^*(t) + \rho_{34}^*\Omega f_3^*(t)]/2, \\ \dot{\tilde{\rho}}_{24} &= i[(i\Gamma + 2\pi\Delta)\tilde{\rho}_{24} + (\rho_{44} - \rho_{22})\Omega f_4^*(t) - \tilde{\rho}_{12}^*\Omega f_3^*(t) - \rho_{34}\Omega f_2^*(t)]/2, \\ \dot{\tilde{\rho}}_{23} &= i[(i\Gamma + 2\pi\Delta)\tilde{\rho}_{23} - (\rho_{33} - \rho_{22})\Omega f_2^*(t) - \tilde{\rho}_{12}^*\Omega f_1^*(t) + \rho_{34}^*\Omega f_4^*(t)]/2, \\ \dot{\tilde{\rho}}_{12} &= i[(i\gamma_2 - 4\pi\Delta)\tilde{\rho}_{12} + \tilde{\rho}_{23}^*\Omega f_1^*(t) + \tilde{\rho}_{13}\Omega f_2(t) + \tilde{\rho}_{24}^*\Omega f_3^*(t) - \tilde{\rho}_{14}\Omega f_4(t)]/2, \\ \dot{\tilde{\rho}}_{34} &= i[2i\gamma_{43}\rho_{34} - \tilde{\rho}_{23}^*\Omega f_4^*(t) - \tilde{\rho}_{13}^*\Omega f_3^*(t) - \tilde{\rho}_{24}\Omega f_2(t) + \tilde{\rho}_{14}\Omega f_1(t)]/2. \end{aligned} \quad (\text{A12})$$

Here, we assume a solution for the off-diagonal matrix elements of the form $\rho_{13(4)} = \tilde{\rho}_{13(4)}e^{i\omega_{+/-}t}$, $\rho_{23(4)} = \tilde{\rho}_{23(4)}e^{i\omega_{-/-}t}$, and $\rho_{12} = \tilde{\rho}_{12}e^{i\omega_{+-/-}t}$, where $\omega_{+-} = \omega_+ - \omega_-$, and apply the secular approximation. γ_1 and γ_2 are the decay rates of the ground-state population and the coherence, respectively. Similarly, Γ is the decay rate of the population from excited state $|3\rangle$ ($|4\rangle$) to the ground state, and $\gamma_{31}(\gamma_{32})$ and $\gamma_{41}(\gamma_{42})$ are the decay rates of the coherence from excited states $|3\rangle$ and $|4\rangle$ to the ground state, respectively. γ_{43} is the coherence decay rate between $|4\rangle$ and $|3\rangle$. In typical experiments, we presume that $\gamma_1 = \gamma_2$, $\gamma_{31} = \gamma_{32} = \gamma_{41} = \gamma_{42} = \Gamma/2$, and $\gamma_{43} = \Gamma/2000$.

We use the following notation: $\nu_i = \omega_i/(2\pi)$ for $i = 1-4$, $\nu_{+/-} = \omega_{+/-}/(2\pi)$, $\nu_{+-} = \omega_{+-}/(2\pi)$, $\nu_{\text{hf}} = \nu_2 - \nu_1$, $\nu_{43} = \nu_4 - \nu_3$, $\nu_{31(2)} = \nu_3 - \nu_{1(2)}$, and $\nu_{41(2)} = \nu_4 - \nu_{1(2)}$. The two-photon detuning (Raman detuning) is $\Delta = \Delta_1 - \Delta_2 = \nu_{+-} - \nu_{\text{hf}}$ and the single-photon detuning are $\Delta_{1(2)} = \nu_{+/-} - \nu_{31(2)}$ and $\Delta_{3(4)} = \nu_{+/-} - \nu_{41(2)}$. For ease of discussion, we assume that $|3\rangle$ and $|4\rangle$ are degenerate ($\nu_{43} = 0$), which means that $\Delta_3 = \Delta_1$ and $\Delta_4 = \Delta_2$. In our case, where the bichromatic light is obtained by direct modulation of a DBR laser diode at half the ground-state splitting frequency, we have the relation $\Delta_1 = -\Delta_2 = \Delta/2$.

The initial conditions are

$$\begin{aligned} \rho_{11}(t=0) &= \rho_{22}(t=0) = 0.5, \\ \rho_{33}(t=0) &= \rho_{44}(t=0) = 0, \\ \tilde{\rho}_{12}(t=0) &= \tilde{\rho}_{13}(t=0) = \tilde{\rho}_{14}(t=0) = \end{aligned}$$

$$\tilde{\rho}_{23}(t=0) = \tilde{\rho}_{24}(t=0) = \rho_{34}(t=0) = 0. \quad (\text{A13})$$

4. Susceptibilities of the atomic medium

For the probe stage, the expressions for the susceptibilities of the atomic medium are $\chi_{\omega_+}^\pm = \eta \rho_{3(4)1}$ and $\chi_{\omega_-}^\pm = \mp \eta \rho_{3(4)2}$, in which $\eta = 2N_a d/\varepsilon_0 E_{\text{probe}}$, where N_a is the atom density. Thus, we have $\beta_{\omega_+} = \pi L \eta \operatorname{Re}(\rho_{13} - \rho_{14})/2\lambda_{\omega_+}$, $\beta_{\omega_-} = -\pi L \eta \operatorname{Re}(\rho_{23} + \rho_{24})/2\lambda_{\omega_-}$, $\alpha_{\omega_+}^\pm = -2\pi \eta \operatorname{Im}(\rho_{13(4)})/\lambda_{\omega_+}$, and $\alpha_{\omega_-}^\pm = \pm 2\pi \eta \operatorname{Im}(\rho_{23(4)})/\lambda_{\omega_-}$. Substituting the results obtained from the density matrix [Eq. (A12)] into Eqs. (A8) and (A9), we then obtain the results shown in Fig. 2.

- [1] S. E. Harris, J. E. Field, and A. Imamoglu, Nonlinear Optical Processes Using Electromagnetically Induced Transparency, *Phys. Rev. Lett.* **64**, 1107 (1990).
- [2] G. Alzetta, A. Gozzini, L. Moi, and G. Orriols, An experimental method for the observation of r.f. transitions and laser beat resonances in oriented Na vapour, *Nuovo Cimento Soc. Ital. Fis.* **36B**, 5 (1976).
- [3] R. M. Whitley, C. R. Stroud Jr., Double optical resonance, *Phys. Rev. A* **14**, 1498 (1976).
- [4] R. Wynands and A. Nagel, Precision spectroscopy with coherent dark states, *Appl. Phys. B* **68**, 1 (1999).
- [5] E. Arimondo, Coherent population trapping in laser spectroscopy, *Prog. Opt.* **35**, 257 (1996).
- [6] P. Yun, F. Tricot, C. E. Calosso, S. Micalizio, B. Francois, R. Boudot, S. Guérardel, and E. de Clercq, High-Performance Coherent Population Trapping Clock with

- Polarization Modulation, *Phys. Rev. Appl.* **7**, 014018 (2017).
- [7] X. Liu, E. Ivanov, V. I. Yudin, J. Kitching, and E. A. Donley, Low-Drift Coherent Population Trapping Clock Based on Laser-Cooled Atoms and High-Coherence Excitation Fields, *Phys. Rev. Appl.* **8**, 054001 (2017).
- [8] M. Abdel Hafiz, G. Coget, M. Petersen, C. E. Calosso, S. Guérandel, E. De Clercq, and R. Boudot, Symmetric autabalanced Ramsey interrogation for high-performance coherent population-trapping vapor-cell atomic clock, *Appl. Phys. Lett.* **112**, 244102 (2018).
- [9] P. Yun, Q. Li, Q. Hao, G. Liu, E. de Clercq, S. Guérandel, X. Liu, S. Gu, Y. Gao, and S. Zhang, High-performance coherent population trapping atomic clock with direct-modulation distributed Bragg reflector laser, *Metrologia* **58**, 054001 (2021).
- [10] J. Kitching, Chip-scale atomic devices, *Appl. Phys. Rev.* **5**, 031302 (2018).
- [11] M. Abdel Hafiz, G. Coget, E. de Clercq, and R. Boudot, Doppler-free spectroscopy on the Cs D_1 line with a dual-frequency laser, *Opt. Lett.* **41**, 2982 (2016).
- [12] D. Brazhnikov, M. Petersen, G. Coget, N. Passilly, V. Maurice, C. Gorecki, and R. Boudot, Dual-frequency sub-Doppler spectroscopy: Extended theoretical model and microcell-based experiments, *Phys. Rev. A* **99**, 062508 (2019).
- [13] A. Gusching, M. Petersen, N. Passilly, M. Abdel Hafiz, E. de Clercq, and R. Boudot, Short-term stability of Cs microcell-stabilized lasers using dual-frequency sub-Doppler spectroscopy, *J. Opt. Soc. Am. B* **38**, 3254 (2021).
- [14] P. D. D. Schwindt, S. Knappe, V. Shah, L. Hollberg, and J. Kitching, Chip-scale atomic magnetometer, *Appl. Phys. Lett.* **85**, 6409 (2004).
- [15] A. Aspect, E. Arimondo, R. Kaiser, N. Vansteenkiste, and C. Cohen-Tannoudji, Laser Cooling below the One-Photon Recoil Energy by Velocity-Selective Coherent Population Trapping, *Phys. Rev. Lett.* **61**, 826 (1988).
- [16] A. V. Taichenachev, A. M. Tumaykin, and V. I. Yudin, Quantum theory of cooling of atoms below the one-photon recoil energy by a pulsed field, *JETP Lett.* **65**, 779 (1997).
- [17] M. Fleishhauer and M. D. Lukin, Dark-State Polaritons in Electromagnetically Induced Transparency, *Phys. Rev. Lett.* **84**, 5094 (2000).
- [18] M. Bajesy, A. S. Zibrov, and M. D. Lukin, Stationary pulses of light in an atomic medium, *Nature* **426**, 638 (2003).
- [19] A. M. Akulshin, S. Barreiro, and A. Lezama, Electromagnetically induced absorption and transparency due to resonant two-field excitation of quasi-degenerate levels in Rb vapor, *Phys. Rev. A* **57**, 2996 (1998).
- [20] A. V. Taichenachev, A. M. Tumaykin, and V. I. Yudin, Electromagnetically induced absorption in a four-state system, *Phys. Rev. A* **61**, 011802(R) (1999).
- [21] C. Affolderbach, S. Knappe, R. Wynands, A. V. Taichenachev, and V. I. Yudin, Electromagnetically induced transparency and absorption in a standing wave, *Phys. Rev. A* **65**, 043810 (2002).
- [22] D. V. Brazhnikov, S. Ignatovich, V. I. Vishnyakov, R. Boudot, and M. N. Skvortsov, Electromagnetically induced absorption scheme for vapor-cell atomic clock, *Opt. Exp.* **27**, 36034 (2019).
- [23] L. Lenci, L. Marmugi, F. Renzoni, S. Gozzini, A. Lucchesini, and A. Fioretto, Time-domain Ramsey-narrowed sub-kHz electromagnetically induced absorption in atomic potassium, *J. Phys. B: At. Mol. Opt. Phys.* **52**, 085002 (2019).
- [24] J. Vanier, Atomic clocks based on coherent population trapping: A review, *Appl. Phys. B* **81**, 421 (2005).
- [25] Y. Y. Jau, E. Miron, A. B. Post, N. N. Kuzma, and W. Happer, Push-Pull Optical Pumping of Pure Superposition States, *Phys. Rev. Lett.* **93**, 160802 (2004).
- [26] X. Liu, J. M. Merolla, S. Guérandel, C. Gorecki, E. de Clercq, and R. Boudot, Coherent-population-trapping resonances in buffer-gas-filled Cs-vapor cells with push-pull optical pumping, *Phys. Rev. A* **87**, 013416 (2013).
- [27] T. Zanon, S. Guérandel, E. De Clercq, D. Holleville, N. Dimarcq, and A. Clairon, High Contrast Ramsey Fringes with Coherent-Population-Trapping Pulses in a Double Lambda Atomic System, *Phys. Rev. Lett.* **94**, 193002 (2005).
- [28] A. V. Taichenachev, V. I. Yudin, V. L. Velichansky, and S. A. Zibrov, On the unique possibility of significantly increasing the contrast of dark resonances on the D_1 line of Rb-87, *JETP Lett.* **82**, 398 (2005).
- [29] S. V. Kargapoltev, J. Kitching, L. Hollberg, A. V. Taichenachev, V. L. Velichansky, and V. I. Yudin, High-contrast dark resonance in $\sigma^+ - \sigma^-$ optical field, *Laser Phys. Lett.* **1**, 495 (2004).
- [30] X. Liu, V. I. Yudin, A. V. Taichenachev, J. Kitching, and E. A. Donley, High contrast dark resonances in a cold-atom clock probed with counterpropagating circularly polarized beams, *Appl. Phys. Lett.* **111**, 224102 (2017).
- [31] A. V. Taichenachev, V. I. Yudin, V. L. Velichansky, A. S. Zibrov, and S. A. Zibrov, Pure superposition states of atoms generated by a bichromatic elliptically polarized field, *Phys. Rev. A* **73**, 013812 (2006).
- [32] P. Yun, J. M. Danet, D. Holleville, E. de Clercq, and S. Guérandel, Constructive polarization modulation for coherent population trapping clock, *Appl. Phys. Lett.* **105**, 31106 (2014).
- [33] Y. Yano and S. Goka, High-contrast coherent population trapping based on crossed polarizers method, *IEEE Trans. Ultrason. Ferroelec. Freq. Contr.* **61**, 1953 (2014).
- [34] M. Rosenbluh, V. Shah, S. Knappe, and J. Kitching, Differentially detected coherent population trapping resonances excited by orthogonally polarized laser fields, *Opt. Express* **14**, 6588 (2006).
- [35] V. Gerginov, S. Knappe, V. Shah, L. Hollberg, and J. Kitching, Laser noise cancellation in single-cell CPT clocks, *IEEE Trans. Instrum. Meas.* **57**, 1357 (2008).
- [36] B. Tan, Y. Tian, H. Lin, J. Chen, and S. Gu, Noise suppression in coherent population trapping atomic clock by differential magneto-optic rotation detection, *Opt. Lett.* **40**, 3703 (2015).
- [37] F. Riehle, Frequency Standards: Basics and Applications, Wiley-VCH, Weinheim, chap 3, p. 77, 2004.
- [38] Y. Tian, B. Z. Tan, J. Yang, Y. Zhang, and S. H. Gu, Ramsey-CPT spectrum with the Faraday effect and its application to atomic clocks, *Chin. Phys. B* **24**, 063302 (2015).

- [39] M. Abdel Hafiz and R. Boudot, A coherent population trapping Cs vapor cell atomic clock based on push-pull optical pumping, *J. Appl. Phys.* **118**, 124903 (2015).
- [40] M. Abdel Hafiz, G. Coget, P. Yun, S. Guérandel, E. de Clercq, and R. Boudot, A high-performance Raman-Ramsey Cs vapor cell atomic clock, *J. Appl. Phys.* **121**, 104903 (2017).
- [41] J. M. Danet, M. Lours, P. Yun, S. Guérandel, and E. de Clercq, Frequency instability investigations on a Cs cell clock based on pulsed coherent population trapping, 2013 Joint UFFC, EFTF and PFM Symposium.
- [42] C. P. Pearman, C. S. Adams, S. G. Cox, P. F. Griffin, D. A. Smith, and I. G. Hughes, Polarization spectroscopy of a closed atomic transition: Applications to laser frequency locking, *J. Phys. B* **35**, 5141 (2002).
- [43] B. Wang, S. Li, J. Ma, H. Wang, K. C. Peng, and M. Xiao, Controlling the polarization rotation of an optical field via asymmetry in electromagnetically induced transparency, *Phys. Rev. A* **73**, 051801(R) (2006).
- [44] S. Li, B. Wang, X. Yang, Y. Han, H. Wang, M. Xiao, and K. C. Peng, Controlled polarization rotation of an optical field in multi-Zeeman-sublevel atoms, *Phys. Rev. A* **74**, 033821 (2006).